EARTHQUAKE ENGINEERING AND STRUCTURAL DYNAMICS
Earthquake Engng Struct. Dyn. 2011; **40**:1083–1102
Published online 22 October 2010 in Wiley Online Library (wileyonlinelibrary.com). DOI: 10.1002/eqe.1071

A novel type of angle steel buckling-restrained brace: Cyclic behavior and failure mechanism

Junxian Zhao[1], Bin Wu[1,*,†] and Jinping Ou[1,2]

[1]*School of Civil Engineering, Harbin Institute of Technology, Harbin 150090, People's Republic of China*
[2]*School of Civil and Hydraulic Engineering, Dalian University of Technology, Dalian 116024, People's Republic of China*

SUMMARY

A novel type of angle steel buckling-restrained brace (ABRB) has been developed for easier control on initial geometric imperfection in the core, more design flexibility in the buckling restraining mechanism and easier assembly work. The steel core is composed of four angle steels to form a non-welded cruciform shape restrained by two external angle steels, which are welded longitudinally to form an external tube. Component test was conducted on seven ABRB specimens under uniaxial quasi-static cyclic loading. The test results reveal that the consistency between the actual and design behavior of ABRB can be well achieved without the effect of weld in the core. The ABRBs with proper details exhibited stable cyclic behavior and satisfactory cumulative plastic ductility capacity, so that they can serve as effective hysteretic dampers. However, compression–flexure failure at the steel core projection was found to be the primary failure mode for the ABRBs with hinge connections even though the cross-section of the core projection was reinforced two times that of the yielding segment. The failure mechanism is further discussed by investigating the N_u–M_u correlation curve. It is found that the bending moment response developed in the core projection induced by end rotation was the main cause for such a failure mode, and it is suggested that core projection should be kept within elastic stage under the possible maximum axial load and bending moment response. Copyright © 2010 John Wiley & Sons, Ltd.

Received 17 February 2010; Revised 28 August 2010; Accepted 30 August 2010

KEY WORDS: buckling-restrained brace; hysteretic damper; angle steel; cyclic behavior; compression-flexure failure; brace end rotation

1. INTRODUCTION

Buckling-restrained braces are one kind of yielding metallic dampers, which have become increasingly popular in seismic-prone areas for their stable cyclic behavior and excellent energy dissipation capacity. A detailed summary of the studies on the seismic behavior of BRBs conducted in Asia has been reported by Xie [1], and the studies on BRB frame systems at the component, subassemblage and frame level have been summarized by Uang *et al.* [2]. According to the previous researches, the BRBs can be typically categorized into the following three types according to the external restraints: (1) core buckling restrained by steel tube filled with concrete or mortar [3, 4]; (2) core buckling restrained by reinforced concrete panel or member [5–7]; and (3) core buckling restrained by all-steel components [8–12], called all-steel BRB (Figure 1).

The steel core and external restraint of all-steel BRBs are composed of all steel components without concrete or mortar infilled and generally there is no need to paint unbonding material onto

*Correspondence to: Bin Wu, School of Civil Engineering, Harbin Institute of Technology, Harbin 150090, People's Republic of China.
†E-mail: bin.wu@hit.edu.cn

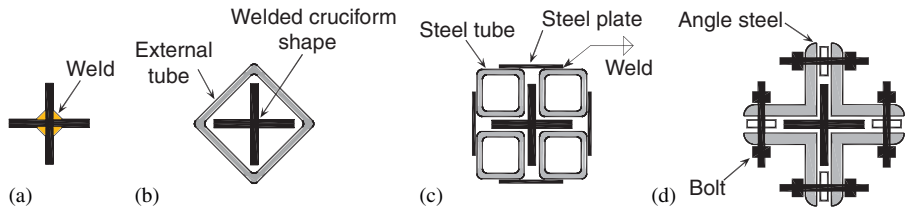

Figure 1. Conventional cross-sections for all-steel BRBs.

the steel core; hence, the all-steel BRBs have the advantages of lighter weight, easier fabrication and easier control on member quality. A welded cruciform shape (Figure 1(a)) is generally employed as the steel core cross-section to facilitate brace-to-gusset plate connection and provide large lateral-resisting force to the main structures. The typical all-steel BRBs with welded cruciform cross-section in the steel core as an energy dissipation part are illustrated in Figure 1(b)–(d), in which the steel core is fabricated by welding three steel plates together when there is no cruciform shaped section steel commercially supplied. Several tests have been conducted to investigate the hysteretic behavior of the all-steel BRBs with welded cruciform shape in the steel core by Murase *et al.* [9], Ma *et al.* [10], Narihara *et al.* [11] and Fukuda *et al.* [12], which showed that the all-steel BRBs exhibited stable and repeatable cyclic behavior. However, several key problems still need to be resolved to ensure higher member quality and proper seismic performance. To this end, a novel type of BRB, called angle steel buckling-restrained brace (ABRB), has been introduced and tested by the authors. This paper will describe the characteristics, component test results and failure mode analysis of the new BRB.

2. PRESENTATION OF NOVEL ABRB

Although all-steel BRBs have been studied by many researchers and applied in practice, some key issues have yet to be addressed as follows:

- *Initial geometric imperfection in the steel core*
  Murase *et al.* [9] found that significant amount of high-temperature welding during the fabrication of steel core with cruciform shape would cause an unexpected residual welding deformation, resulting in a technical difficulties when placing the core into the external tube (Figure 1(b)) especially for long braces.
- *Inconsistency in member behavior*
  Ma *et al.* [10] conducted uniaxial test on two full-scale all-steel BRB specimens illustrated in Figure 1(b), and they found that the actual axial yielding force of such BRB was approximately 40% higher than the computed yielding force based on tensile coupon test, which is primarily due to the additional cross-sectional area and higher yielding stress of the weld in the steel core. Similar results were observed on another type of BRB in the test conducted by Nagao *et al.* [7], in which the steel core was fabricated by welding four steel plates together to form a square hollow tube restrained by a reinforced concrete member. Their test results showed that the actual yielding force of such BRB was 10% higher.
- *Low-cycle fatigue*
  The tests conducted by Narihara *et al.* [11] on the BRBs shown in Figure 1(c) and the tests performed by Ma *et al.* [10] on the BRBs presented in Figure 1(b) indicated that the all-steel BRBs with the effect of welding in the steel core may experience premature rupture, showing undesirable low-cycle fatigue properties. Moreover, similar results were also observed in the component test by Fukuda *et al.* [12] on the BRB shown in Figure 1(d) and in the subassemblage test by Newell *et al.* [13] on the BRBs with concrete-filled steel tube as restraining part. Their test results showed that the BRBs exhibited relatively poorer low-cycle fatigue property than those without the effect of welding in the steel core.
- Brace–beam–column connection behavior

DOI: 10.1002/eqe

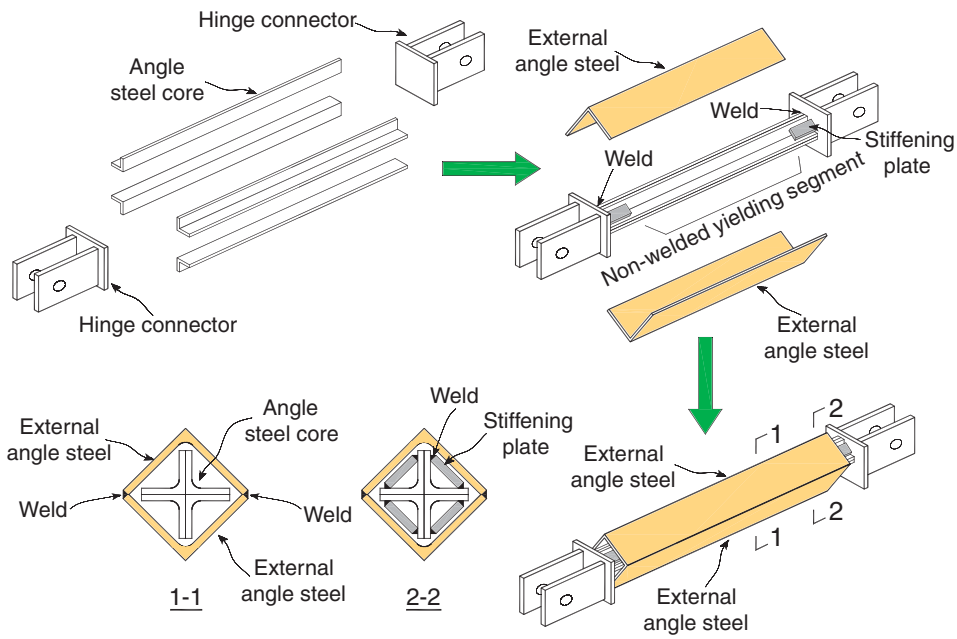

Figure 2. Main components of angle steel BRB.

Aiken *et al.* [14] performed three cyclic tests on a 0.7-scale one-bay one-story buckling-restrained braced frames (BRBF) with bolted brace-to-gusset plate connections. Beam flange fracture and out-of-plane buckling of the gusset plate connections were observed in such frame tests. It revealed that the current rigid brace–beam–column connections may lead to the in-plane and out-of-plane flexural response in the braces and gusset plates, which may detrimentally affect the seismic behavior of the BRBF system.

A novel type of all-steel BRB, called angle steel BRB (ABRB), has been developed based on the problems above. The schematic diagram of the main components of ABRB is presented in Figure 2. As is shown, the steel core of ABRB consists of four combined angle steels to form a non-welded cruciform shape within the yielding segment to minimize initial geometric imperfection, ensure consistency in member quality, and improve its low-cycle fatigue property. Eight stiffening plates are welded to the core ends as stiffening segment to ensure elastic response within these regions. Two hinge connectors are welded to the core ends with full-penetration to minimize the in-plane flexural response in the brace–beam–column connections. Then, the steel core is restrained by two external angle steels which are welded longitudinally to form an external tube. Such an external restraint has the advantages of more design flexibility compared with the BRB in Figure 1(b), less welding compared with the BRB in Figure 1(c), and higher moment of inertia compared with the BRB in Figure 1(d).

The remainder of this paper will describe component test on seven ABRB specimens under uniaxial quasi-static cyclic loading. Then, the seismic performance of the ABRBs as a hysteretic damper is evaluated. Furthermore, the failure mode and the characteristics of brace end rotation of the ABRBs are presented. Finally, the failure mechanism of the primary failure mode is discussed and several design implications are proposed.

3. TEST PROGRAM

Seven ABRB specimens labeled ABRB-1 to ABRB-7 were designed according to the comparative parameters. The configurations and material properties of the ABRB specimens are described first, and then the test cases, test setup and loading protocol.

DOI: 10.1002/eqe

3.1. Configuration of steel core

The constructional details of the steel core specimens are presented in Figure 3, in which the geometric dimensions presented are all design dimensions. The angle steels of the steel core were processed by milling machine (cold processing) without any flame cut to minimize the initial geometric imperfection caused by high temperature. The total design length of the steel core was 756 mm, and the nominal thickness of single angle steel was 5 mm for all the steel core specimens. The design length of the yielding segment was 556 mm, and that of stiffening segment at each end was 100 mm for specimen ABRB-1∼ABRB-4 and ABRB-7. For specimen ABRB-5 and ABRB-6, the design length of the yielding segment and the stiffening segment were changed to 456 and 150 mm, respectively.

Two types of steel core specimens (type A and type B) were designed to investigate the effect of core type detail since few comparisons have ever been made between these two core types to examine such an effect quantitatively. The horizontal limbs of the angle steel were locally enlarged in the middle as a stopper to prevent the external restraint from axially slipping. The geometric shape of the stoppers were fabricated either by abrupt variation (type A) of the cross-sectional dimension in the horizontal limbs or by gradual variation (type B) with the horizontal inclination of approximately 13°. The four angle steels were connected together only in the middle by four small spot weld points and at the locations between the adjacent angle steels within the core stiffening segment (the dashed line and cross-section 2-2 in Figure 3) to improve the co-working behavior of the four angle steels. There was no welding within the rest parts of the core yielding segment.

Both ends of the steel cores were reinforced by welding four stiffening plates at each end to keep it elastic (considering the axial load only) within the core stiffening segment, and a distance of 25 mm was provided between the weld end of the angle steels and that of the stiffening plates to minimize the stress concentration caused by residual welding stress at the end of core yielding segment.

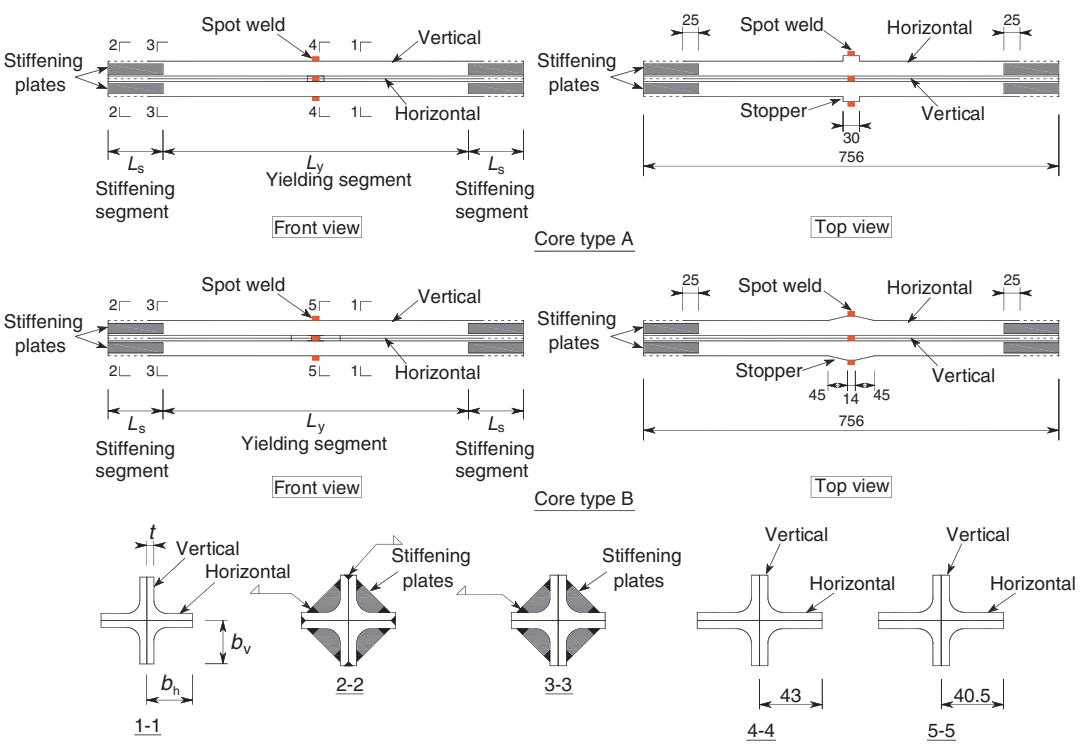

Figure 3. Configuration of steel core specimens.

DOI: 10.1002/eqe

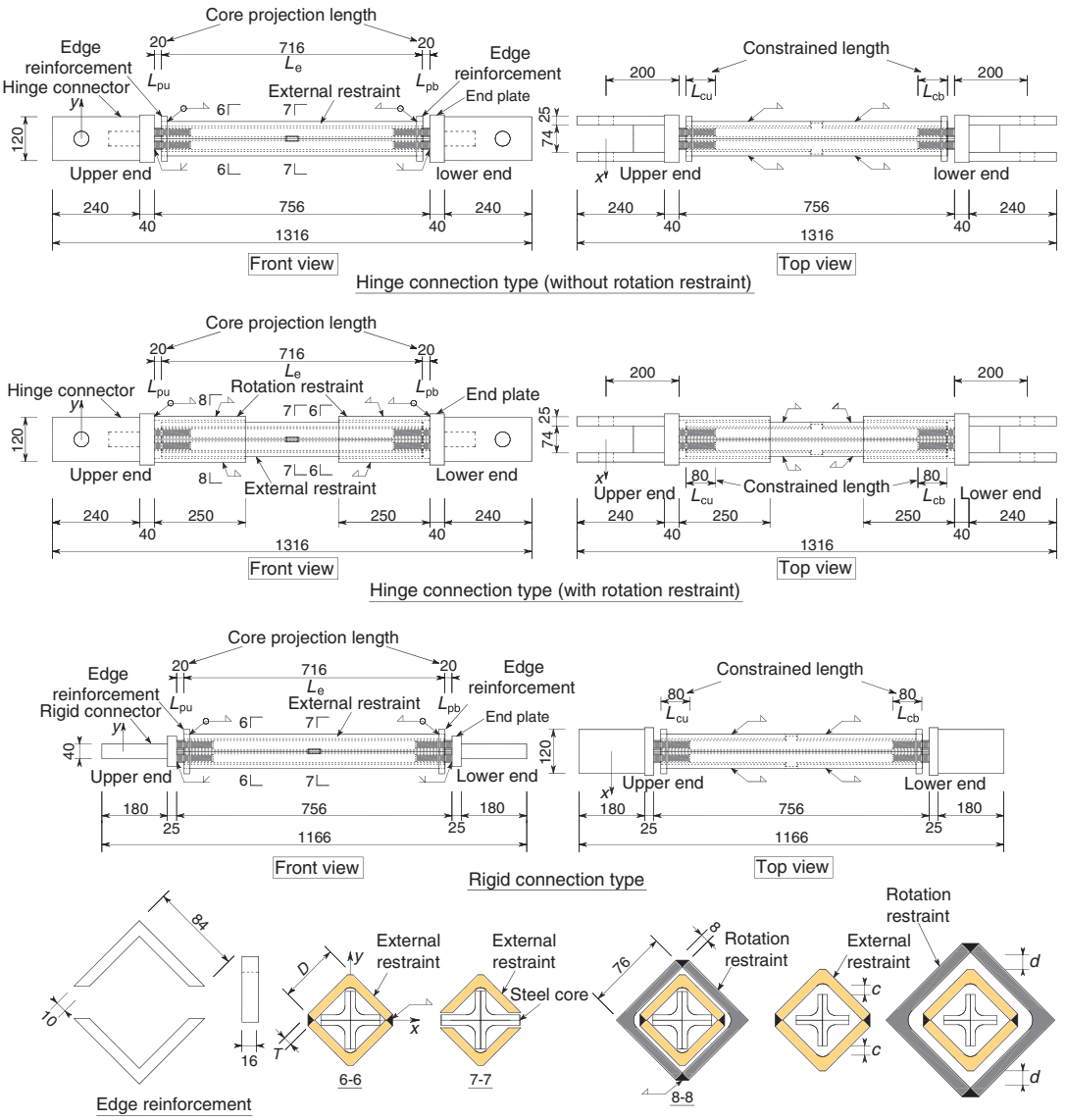

Figure 4. Configuration of ABRB specimens.

3.2. *Configuration of brace end connections and buckling-restraining mechanism*

The constructional details of the connections and buckling-restraining mechanism for three types of ABRB specimens with core type A as an example are presented in Figure 4, in which the geometric dimensions presented are all design dimensions.

Two types of connections, including hinge connection and rigid connection, were designed to examine the effect of brace end rotation. The end of steel core was welded to the end of connections with full-penetration.

The angle steels in the external and rotation restraints were also processed by milling machine. The external restraint comprised two angle steels welded longitudinally to form a square hollow tube, and it had a total design length of 716 mm for all the specimens, which was 40 mm shorter than that of the steel core to accommodate the relative axial deformation in between. The nominal thickness of single angle steel in the external restraint was 8 mm for all the specimens.

The external angle steels were locally cut in the middle on both limbs according to the geometric shape of the core stoppers so as to get themselves stuck by stoppers; hence, the axial slippage of

DOI: 10.1002/eqe

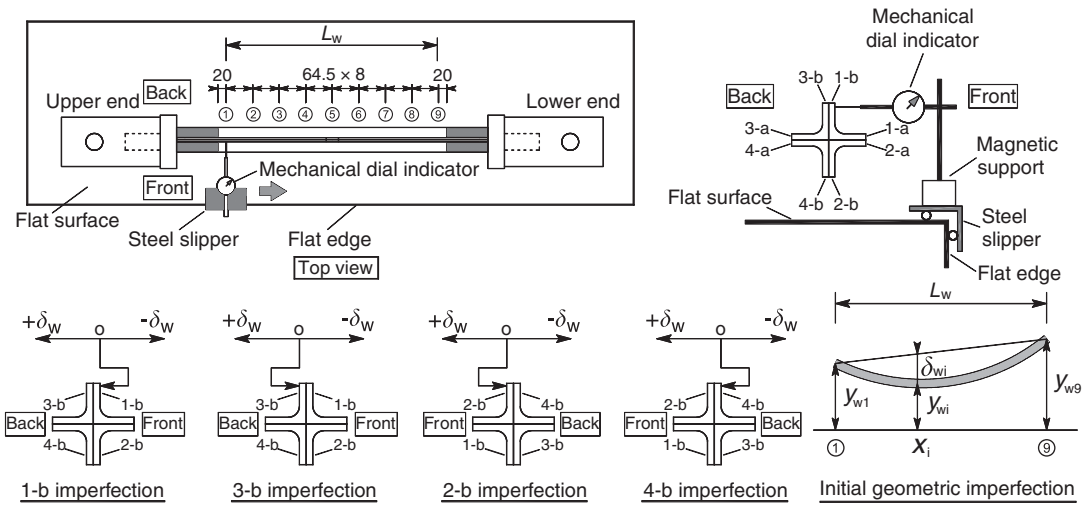

Figure 5. Measurement of initial geometric imperfection in the steel core.

the external restraint can be restricted. A proper clearance was provided between the steel core and the external restraint to accommodate the lateral expansion of the core due to Poisson's effect. The design clearance c was 1 mm on both sides for ABRB-1∼ABRB-5 and ABRB-7, and 2 mm for ABRB-6 by slightly changing the width of the angle steel core. Furthermore, machine oil was painted onto the exterior surface of the steel core and the interior surface of the external restraint to minimize the frictional response in between. Finally, both ends of the external restraint were reinforced by welding two stiffening hoops together to prevent the local failure at the edge of external restraint.

The rotation restraint, inspired by the collar apparatus of the BRBs by Star Seismic Company [15], was designed to restrict the brace end rotation (without edge reinforcement at the end of external restraint for this type). Such a rotation restraint consisted of two short angle steels welded longitudinally to form a short square hollow tube, and the nominal thickness of the angle steels in the rotation restraint was 8 mm. Only one end of the rotation restraint was connected to the end plate of the connectors by fillet weld, and a design clearance with $d = 1$ mm was provided between the rotation restraint and the external restraint. Hence, the brace end rotation can be restricted when the rotation restraint contacts with the external restraint. Moreover, machine oil was also painted onto the contact surface in between to minimize the frictional response.

3.3. Initial geometric imperfection in the steel core

The initial geometric imperfection of the core yielding segment was measured after all the welding related to the steel core was completed and the specimens were naturally cooled. The measurement setup is presented in Figure 5. First, a mechanical dial indicator was placed onto a magnetic support which was fixed on a steel slipper. The slipper was placed in close contact with the flat platform, so that it could be moved horizontally along the flat edge from points No.1 to No.9 with the spacing of 64.5 mm between each measure point. At each measure point, data of y_{wi} from the mechanical dial indicator was recorded down, and the initial geometric imperfection δ_{wi} can be obtained as follows:

$$\delta_{wi} = y_{w1} + (y_{w9} - y_{w1})\frac{x_i}{L_w} - y_{wi} \tag{1}$$

in which x_i is the distance between the ith and the first measuring points.

The representative distribution curves of the relative initial geometric imperfection δ_w/L_w along the measure length L_w at each measure point are shown in Figure 6, and the positive and negative values of δ_w are illustrated in Figure 5 for each angle steel plate, respectively. Note that some of

DOI: 10.1002/eqe

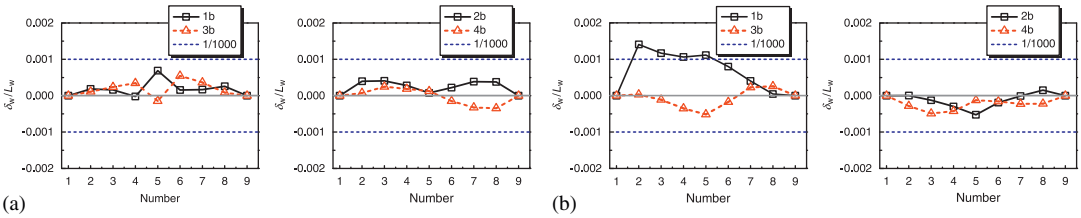

Figure 6. Relative initial geometric imperfections in the steel core: (a) ABRB-1 and (b) ABRB-2.

Table I. Material properties of main steel materials.

Category	Material no.	Steel type	Material grade	Yield stress f_y (MPa)	Tensile strength f_u (MPa)	Elastic modulus E (MPa)	Elongation percentage (%)
Steel core	①	∟50×5	Q235-B	301.0	439.5	1.99×10^5	36.9
	②	∟70×5	Q235-B	303.1	447.6	1.99×10^5	34.4
External	③	∟90×8	Q235-B	256.3	412.6	2.03×10^5	36.3
restraint	④	∟75×8	Q235-B	284.2	447.2	2.01×10^5	33.4
Stiffening	⑤	$-(t=12\,\text{mm})$	Q345-B	364.2	535.4	2.13×10^5	27
plate	⑥	$-(t=12\,\text{mm})$	Q235-B	240	397.9	2.05×10^5	37.1

the initial imperfections of the back-to-back angle steels are illusively seen overlapping each other. This is because there was no welding within the non-welded yielding segment except four weld points in the middle of the stoppers, which led to an unavoidable gap between the back-to-back angle steels within the yielding segment. But the initial geometric imperfections were calculated based on their own reference points 1 and 9 of each steel plate, so that some imperfection diagrams overlap. As is shown, most of the relative initial geometric imperfections were within the limit of 1/1000, and some were even within the limit of 1/2000, indicating that the absence of welding within the core yielding segment can indeed help to minimize the initial geometric imperfection of the core. However, a maximum value of approximately 1/710 was observed only in one of the steel plate labeled 1-b in specimen ABRB-2, which may mainly be related to the unskillful fabrication procedure for such specimen.

3.4. Material properties

The material properties obtained from tensile coupon test are listed in Table I. The Chinese low-carbon structural steel Q235-B with nominal yield stress of 235 MPa was adopted for all the angle steels. Two kinds of structural steel, namely Q345-B with nominal yield stress of 345 MPa and Q235-B, were adopted for the stiffening plates.

3.5. Test cases

The actual measured geometric dimensions and specimen parameters of the ABRB specimens are listed in Tables II and III, respectively, in which the definitions of the geometric parameters are illustrated in Figures 3 and 4. Because of unavoidable error in fabrication, the actual dimensions presented may be slightly different from design.

In Table II, A_y represents the actual cross-sectional area of the core yielding segment. A_s and A_{pe} denote the actual cross-sectional area of the stiffening plates within the stiffening segment (not including angle steels) and the equivalent cross-sectional area of the whole stiffening segment (including angle steels), respectively. A_{pe} can be obtained as follows:

$$A_{pe}=A_y+f_{ys}A_s/f_{yc} \tag{2}$$

DOI: 10.1002/eqe

Table II. Geometric dimensions of ABRB specimens.

	Steel core								External restraint		
Specimens	L_y (mm)	L_s (mm)	b_h (mm)	b_v (mm)	t (mm)	A_y (mm^2)	A_s (mm^2)	A_{pe} (mm^2)	D (mm)	T (mm)	L_e (mm)
ABRB-1	561	98	30.29	29.27	4.57	1031.2	836.9	2043.6	58.16	7.7	717
ABRB-2	561.3	97	30.28	28.92	4.65	1040.1	836.9	2052.6	58.07	7.7	716.5
ABRB-3	561.7	97	30.25	29.39	4.72	1063.9	836.9	2076.4	58.26	7.7	716.9
ABRB-4	556.5	99.7	29.59	29.10	4.60	1049.7	837.6	1712.9	58.05	7.68	716
ABRB-5	457.7	149.3	29.64	29.14	4.62	1054.8	792.6	1682.4	57.96	7.63	716
ABRB-6	456.7	149.5	28.61	28.19	4.57	1008.7	792.6	1636.3	57.97	7.65	716
ABRB-7	556	100	29.93	29.54	4.7	1084.5	815.4	1730.1	58.11	7.65	716

Table III. Comparative parameters of ABRB specimens.

Specimens	Material no.	Core type	Connection type	Rotation restraint	e_i (mm)	A_{pe}/A_y	L_{pu} (mm)	L_{pb} (mm)	c (mm)	L_{cu} (mm)	L_{cb} (mm)	P_{cr}/P_{yc}
ABRB-1	①③⑤	A	H	No	0	1.98	21.5	19	1.47	76.5	79	13.2
ABRB-2	①③⑤	A	H	Yes	0	1.97	21	19	1.12	76	78	13.1
ABRB-3	①③⑤	A	R	No	0	1.95	21	19	0.93	76	78	12.8
ABRB-4	②④⑥	B	H	No	0	1.63	26	14	1.48	74	86	12.46
ABRB-5	②④⑥	B	H	No	2	1.59	24	17	1.39	125	132	12.27
ABRB-6	②④⑥	B	H	No	0	1.62	25	14	2.42	125	136	12.79
ABRB-7	②④⑥	B	R	No	0	1.60	21	19	1.08	79	81	12.41

H: Hinge; R: Rigid.

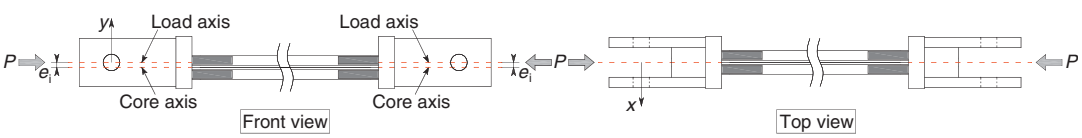

Figure 7. Schematic diagram for initial eccentricity e_i.

where f_{ys} and f_{yc} denote the yield stress of the stiffening plate and the yielding segment obtained by tensile coupon test listed in Table I, respectively.

As is shown in Table III, the initial eccentricity e_i (Figure 7) could be achieved by intentionally moving the core axis away from the load axis of the hinge connectors in the direction of axis y during the assembly of the core to investigate the effect of fabrication error. The core projection length at the upper end (L_{pu}) was larger than that at the lower end (L_{pb}) because of axial clearance in the stopper between the core and the external restraint. This led to somewhat axial slippage of the external restraint when the specimens were placed vertically. This also explains the slightly shorter constrained length of the stiffening segment at the upper end (L_{cu}) than that at the lower end (L_{cb}). The clearance c between the core and external restraint is computed based on the actual measurement, which are slightly different from design. P_{yc} represents the computed axial yielding force by multiplying cross-sectional area A_y and yield stress f_{yc} of the core obtained from tensile coupon test. P_{cr} represents the Euler buckling load (computed with L_e) of the external restraint about axis x (cross-section 6-6 in Figure 4). P_{cr}/P_{yc} denotes the buckling restraining ratio which is a crucial influential factor on the global stability of BRBs, and the test by Watanabe *et al.* [3] showed that it should be no less than 1.5 to ensure global stability. In this study, the buckling restraining ratio was about 13 for all the specimens to prevent them from global buckling during the test.

DOI: 10.1002/eqe

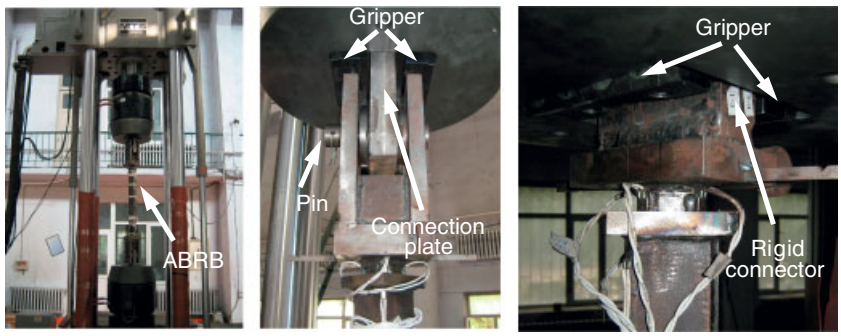

(a) (b) (c)

Figure 8. Test setup and connection details: (a) Testing machine; (b) details for hinge connection; and (c) details for rigid connection.

The comparative parameters of the ABRB specimens Listed in Table III can be grouped into the following two test cases in this study, and the effect of the other specimen parameters will be further discussed in an ongoing companion paper.

(1) Discussion on the effect of core type details
The steel core type (type A for specimen ABRB1–ABRB-3 and type B for the rest of specimens) is varied to investigate the effect of core type details on the low-cycle fatigue property of the core.
(2) Discussion on the effect of brace end rotation
The effect of brace end rotation on the seismic behavior of ABRB is investigated by varying connection type (hinge or rigid) or brace end rotation restraining condition (with or without rotation restraints).

3.6. Test setup

The component test was conducted under uniaxial quasi-static cyclic loading on the MTS electro-hydraulic testing machine with capacity of 2500 kN at the Structural and Seismic Testing Center, Harbin Institute of Technology, China. The elevation view of the test setup is shown in Figure 8(a).

As shown in Figure 8(b) and (c), the specimens with hinge connections were connected to another connection plate at each brace end which were firmly gripped by the MTS machine, whereas the specimens with rigid connections were connected to the testing machine directly.

As shown in Figure 9, two string potentiometers labeled S1 and S2 were mounted between the two end plates of the connectors. The mounting points were located near the steel core ends to measure the axial deformation δ of the specimens (not including the deformation of the connectors). On the other hand, four displacement transducers (LVDT) labeled L1 to L4 were fixed onto the metal supports which were firmly fixed on the ground. The mounting points of LVDTs were located at the end plates of the connectors to measure the upper (L1 and L2) and lower (L3 and L4) brace end rotation, which is shown in Figure 10. The axial force of the specimens was measured by the load cell of the MTS actuator.

3.7. Loading protocol

Two cyclic loading phases, including the elastic phase and the elasto-plastic phase, were imposed on the ABRB specimens. Four cycles were adopted at the force amplitude of approximately $0.6P_{yc}$ of the corresponding specimen under force-controlled method to measure the initial axial stiffness of the ABRBs within elastic stage. When it was completed, another new cyclic loading phase, called elasto-plastic phase, was applied under displacement-controlled method, and all the loading in this phase were started with compression. The loading was imposed at the target core strain

DOI: 10.1002/eqe

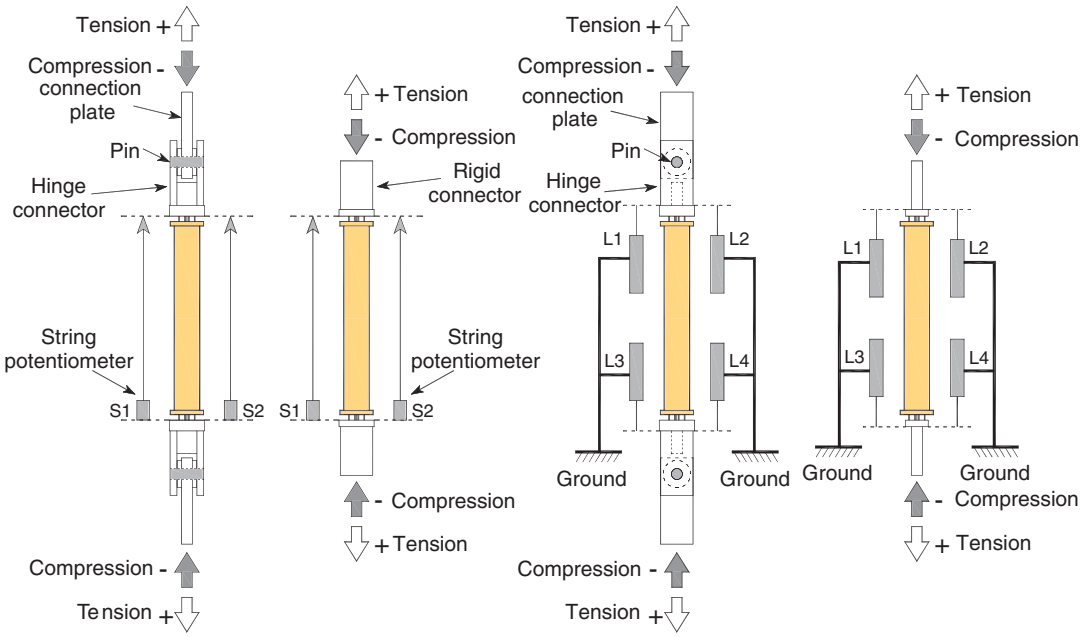

Figure 9. Arrangement of displacement transducers.

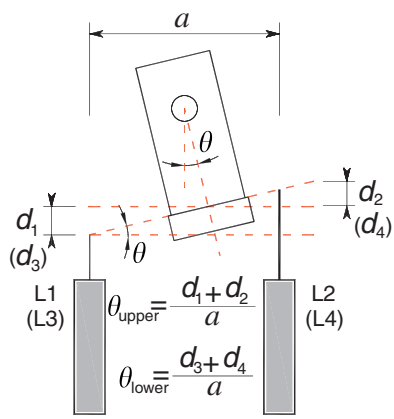

Figure 10. Measurement of brace end rotation demand.

amplitude (deformation of the core δ divided by the length of yielding segment L_y) of 0.4, 0.6, 0.8, 1.0, 1.2, 1.4, 1.6, 1.8, 2.0, 2.2, 2.6 (two cycles each except 1.4%) and 3.0% (keep cyclic loading) until the specimen failed with declined load-bearing capacity.

Six loading cycles at the target core strain of 1.4% was applied to investigate the strength and stiffness degradation behavior of the ABRBs. The core strain of 1.4% corresponds to the inter-story drift of approximately 1/70 for the typical frame model specified in the study by Iwata *et al.* [4] where the BRB is installed into the frame with a horizontal inclination of 45° and with the core yielding length of half the total brace length. The story drift of 1/70 is also the drift limit under severe earthquake ground motion specified in the Technical Specification for Steel Structure of Tall Buildings [16]. In addition, 3% was chosen as the maximum target core strain in the test because the core strain generally remains within the range of 1–2% under severe earthquake ground motion [17].

DOI: 10.1002/eqe

4. TEST RESULTS

4.1. Hysteretic response

The hysteretic loops with non-dimensional axial force P/P_{yc} and actual core strain ε for all the ABRB specimens are presented in Figure 11, in which the shaded triangles denote the decline of load-bearing capacity, indicating specimen failure. Somewhat differences between the actual and target core strain for the ABRBs with hinge connections could be observed, because the displacement of the actuator was taken as the controlled displacement during the test. Hence, the actual core strains obtained by the axial deformation of the steel core would be slightly less than the target ones when the brace ends of hinge-connected specimens rotated.

As is shown, the hysteretic responses of the specimens behaved perfectly linearly within elastic stage. After the braces yielded, most of the specimens exhibited stable and repeatable cyclic behavior within the core strain of 2% without visible strength or stiffness degradation before specimen failure. Specimen ABRB-5 exhibited stable cyclic behavior only within the core strain of approximately 1.2% because of an initial eccentricity was provided for such a specimen. On the other hand, specimen ABRB-7 exhibited the most excellent cyclic behavior within the core strain of 3%. It showed a slight stiffness degradation behavior at the 3% cyclic loading from the compression to tension excursion, but the maximum tension force still remained unchanged. This may be mainly due to the fact that the cumulative residual flexural deformation concentrated significantly on the high mode buckling steel plates under cyclic loading, and they could not be stretched to its original shape even under the same tensile core strain. Hence, somewhat stiffness degradation could be observed during the tension excursion.

4.2. Seismic performance evaluation

The primary seismic performance indices of the ABRB specimens are presented in Table IV. The seismic performance of ABRBs can be evaluated primarily by the following indices, namely initial axial stiffness ratio K_c/K_e, axial yielding force ratio P_{yc}/P_y, axial yielding deformation ratio δ_{yc}/δ_y, compression strength adjustment factor β, ductility μ, cumulative plastic ductility (CPD) and cumulative plastic energy (CPE) dissipation ratio.

(1) Initial axial stiffness ratio K_c/K_e

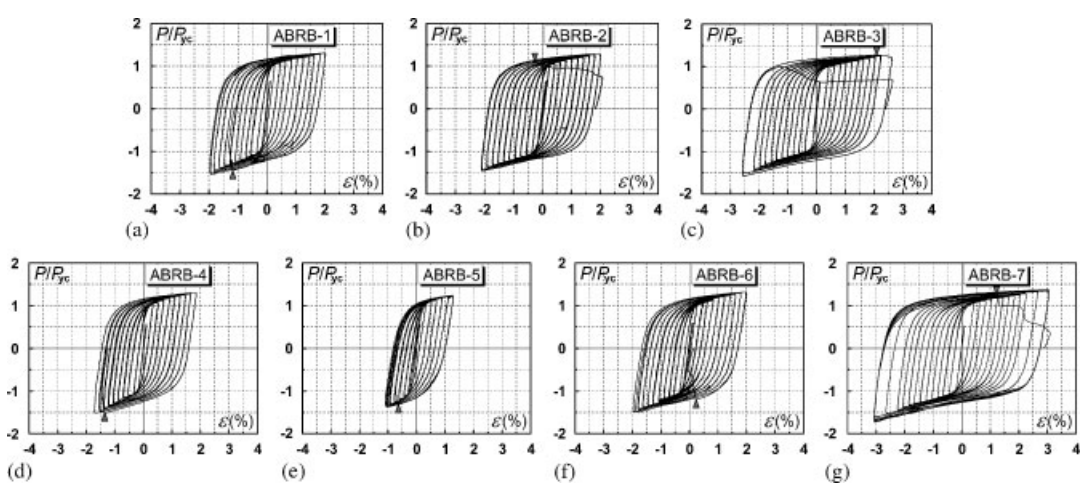

Figure 11. Hysteretic response of ABRB specimens.

DOI: 10.1002/eqe

Table IV. Primary seismic performance indices of ABRB specimens.

Specimen	K_e (kN/mm)	K_c/K_e	P_y (kN)	P_{yc}/P_y	δ_y (mm)	δ_{yc}/δ_y	β	ε_t (%)	ε_c (%)	μ_t	μ_c	CPD	CPE
ABRB-1	302.5	1.02	298.9	1.04	1.04	0.97	1.18	2.04	−1.98	11.4	11.1	539.8	552.7
ABRB-2	299.4	1.04	326.2	0.96	1.16	0.87	1.10	2.02	−2.12	11.3	11.8	518	524.3
ABRB-3	316.9	1.02	310	1.03	1.03	0.98	1.14	2.24	−2.57	12.1	14.3	646	653.1
ABRB-4	303.6	1.04	295.4	1.08	0.93	1.09	1.17	1.87	−1.72	10.3	9.5	417.8	423.1
ABRB-5	335.9	1.00	307.5	1.04	1.05	0.91	1.12	1.29	−1.09	6.2	5.3	179.6	171.9
ABRB-6	307.4	1.05	295.5	1.03	1.01	0.93	1.14	2.01	−1.98	9.8	9.6	442.6	443.3
ABRB-7	303.2	1.07	326.9	1.01	1.17	0.87	1.26	3.06	−3.07	16.8	16.8	1068.2	1153.6
Average	—	1.03	—	1.03	—	0.95	—	—	—	—	—	—	—

ε_t and ε_c denote the peak core strain in tension and compression before specimen failure, respectively.

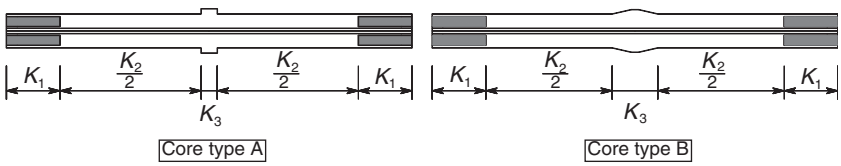

Figure 12. Definition of the initial axial stiffness of the core.

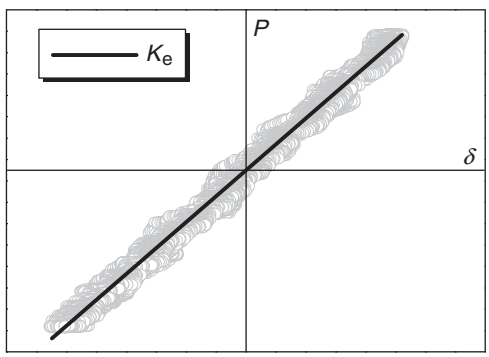

Figure 13. Linear regression of K_e.

K_c and K_e in Table IV denote the theoretically computed initial axial stiffness of the core and experimentally tested initial axial stiffness of the specimens during elastic stage, respectively. K_c can be obtained as follows:

$$K_c = \frac{1}{2/K_1 + 4/K_2 + 1/K_3} \tag{3}$$

where the definition of the parameters is shown in Figure 12. K_1, K_2 and K_3 represent the theoretically computed initial axial stiffness of stiffening segment, yielding segment and stopper segment, respectively. K_e is obtained by linear regression of the hysteretic curve within elastic stage, which is shown in Figure 13. As can be seen from Table IV, K_c agrees well with K_e with an average difference of 3%, indicating that the contribution of frictional response between the steel core and external restraint can be neglected during elastic stage, and the ABRBs will behave as conventional braces under minor earthquake ground motion.

(2) Axial yielding force ratio P_{yc}/P_y and yielding deformation ratio δ_{yc}/δ_y

P_{yc} and P_y in Table IV represent the computed and the experimentally tested axial yielding force, respectively. δ_{yc} and δ_y denote the computed and experimentally tested axial

DOI: 10.1002/eqe

yielding deformation, respectively. P_{yc} and δ_{yc} can be obtained as follows:

$$P_{yc} = f_{yc} A_y \tag{4}$$

$$\delta_{yc} = \varepsilon_{yc} L_y + \frac{2 P_{yc} L_1}{E(A_y + A_s)} \tag{5}$$

As is shown in Table IV, P_{yc} matches well with P_y with an average difference of 3%, and δ_{yc} also agrees well with δ_y with an average difference of 5%, which show that the yielding force and yielding deformation of ABRBs can be successfully predicted on the average level without the effect of welding in the core yielding segment; hence, the consistency between design and actual member behavior of ABRBs can be well achieved.

(3) Compression strength adjustment factor β

The unbalanced response of brace resistance can be evaluated by β, which is presented as follows:

$$\beta = \max\left(\frac{P^i_{\max}}{T^i_{\max}}\right) \tag{6}$$

where $P^i_{\max}$ and $T^i_{\max}$ represent the maximum tension and compression force at the same strain amplitude of the ith cycle before failure, respectively. As is presented in Table IV, the maximum β value of the specimens at the core strain of approximately 2 and 3% equals to 1.18 and 1.26, respectively, and such strain level correspond to the inter-story drift of 1/50 and 1/33, respectively, in the typical frame model by Iwata *et al.* [4]. This shows that the unbalance response of the brace resistance of ABRBs meets the requirement ($\beta \leqslant 1.3$) provided in the AISC Seismic Provision [18].

(4) Ductility μ, CPD and CPE

The definition of ductility μ, CPD and CPE dissipation ratio are presented as follows:

$$\mu_{t,c} = \frac{|\delta_{\text{tmax,cmax}}|}{\delta_{yc}} \tag{7}$$

$$\text{CPD} = \sum [2(|\delta_{\text{tmax}}|_i + |\delta_{\text{cmax}}|_i)/\delta_{yc} - 4] \tag{8}$$

$$\text{CPE} = \frac{\int P\,\mathrm{d}\delta}{2 \times \dfrac{P_{yc}\delta_{yc}}{2}} = \frac{\int P\,\mathrm{d}\delta}{P_{yc}\delta_{yc}} \tag{9}$$

where δ_{tmax} and δ_{cmax} represent the maximum tension and compression axial deformation before specimen failure, respectively. $|\delta_{\text{tmax}}|_i$ and $|\delta_{\text{cmax}}|_i$ represent the maximum tension and compression axial deformation at the ith cycle before specimen failure, respectively. The CPD index represents the cumulative ductility excluding the elastic portion before failure [13], and it is specified in the AISC Seismic Provisions [18] that the CPD index should be no less than 200. The CPE index represents the cumulative plastic energy enclosed by the hysteretic loops divided by the elastic strain energy before failure [4].

According to the nonlinear dynamic analysis by Iwata *et al.* [19] on a ten-story dual system combining moment-resisting frames and buckling-restrained braced frames, the average peak demands of the index of μ, CPD and CPE of the BRBs were 7.2, 109.2 and 98.9, respectively, under the L2 level seismic input ground motion (with average peak ground acceleration of 403 cm/s^2). For L4 level (with average peak ground acceleration of 806 cm/s^2), the corresponding demands were 16.3, 291.5 and 310.8, respectively. The seismic capacities of the ABRB specimens along with the corresponding peak demands are shown in Figure 14. It is clear that the seismic capacities of most of the ABRB specimens exceeded the seismic demands of the L2 level. In addition, the seismic capacities of specimen ABRB-7 exceeded the seismic demands of the L4 level. These show that the ABRBs can exhibit satisfactory seismic performance, so they can serve as effective

DOI: 10.1002/eqe

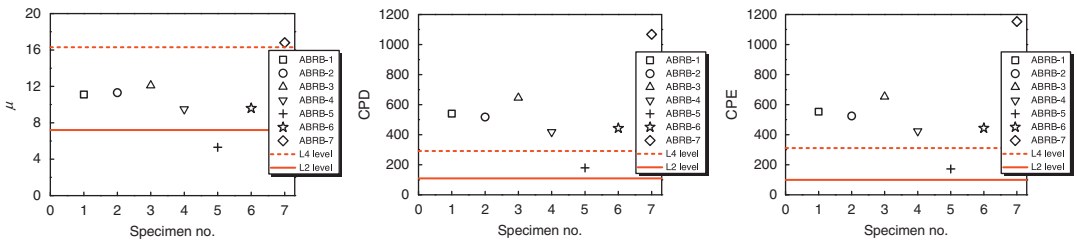

Figure 14. Seismic capacity of ABRB specimens.

hysteretic dampers. In addition, comparison between the ABRB and the BRBs with welded cruciform shape as the cross-section of the core [10, 12, 20] shows that higher core strain and CPD value can be achieved in the ABRBs, indicating that the low-cycle fatigue property of the steel core can be improved without the effect of welding.

4.3. Failure modes

The failure modes of the ABRB specimens can be grouped into two types, including core rupture near the varied cross-section of the stoppers (ABRB-2, ABRB-3, ABRB-7) and compression-flexure failure at the upper steel core projection (ABRB-1ABRB-4∼ABRB-6). No global buckling or local failure at the end of the external restraint was observed during the test. The detailed description of the failure modes is listed in Table V, in which the core strains listed are actual ones. Although core projection failure only occurred at the upper brace end, somewhat residual flexural deformation at the lower core projection could still be observed. The core projection failure mode can also be divided into two types according to the final brace end rotation direction at the moment of failure. As is presented, rotation model C indicates that one of the brace ends rotates in a different direction from the other (one is clockwise and the other is counterclockwise), and rotation model S indicates the upper and lower brace end both have the same rotation direction (both clockwise or counterclockwise).

4.4. Brace end rotation demand

The brace end rotation demand θ versus core strain ε relationship at the first compression peak of each strain amplitude is presented for all the specimens in Figure 15, in which θ_u and θ_b represent the rotation demand of upper and lower brace ends, respectively. The rotation demands at the instant of core projection failure (decline of compressive load bearing capacity) are marked with dashed squares. The rotation demand of ABRB-1 ended at an early core strain of approximately 1.5% before specimen failure because of an unexpected acquisition error in the testing system for LVDTs during the test. The positive and negative values of θ represent the clockwise and counterclockwise rotation directions, respectively, which are consistent with those shown in Table V.

The main features of such rotation demands are presented as follows:

(1) The rotation demands of the rigid-type specimen (ABRB-3 and ABRB-7) were close to zero, which could be negligible compared with those of the hinge type specimens (ABRB-1ABRB-2 and ABRB-4∼ABRB-6).
(2) The rotation demands of the hinge-type specimen ABRB-2 with rotation restraint developed more slowly with the steadily increased strain amplitude than the other hinge-type specimens without rotation restraint (ABRB-1ABRB-4∼ABRB-6). The rotation simply kept constant after the core strain reached 1.5% for ABRB-2. In addition, the absolute amplitudes of the rotation demands of ABRB-2 were also much less than those of the other hinge-type specimens.
(3) At early core strain, the rotation demands of the hinge-type specimen ABRB-1, ABRB-2 and ABRB-4∼ABRB-6 developed more significantly before a certain core strain (marked with dashed circle), and they developed relatively less significantly afterwards until core projection failed at a large rotation demand.

DOI: 10.1002/eqe

Table V. Failure modes of ABRB specimens.

Specimen	Global view of final failure mode	Local enlargement	Failure mode	Final rotation model	Decline of load bearing capacity
ABRB-1			Upper core projection failure	S	At −1.18% in the 1st 2% compression excursion
ABRB-2			Core rupture	—	At −0.25% in the 2nd 2% tension excursion
ABRB-3			Core rupture	—	At 2.05% in the 1st 2.6% tension excursion
ABRB-4			Upper core projection failure	S	At −1.35% in the 2nd 1.8% compression excursion
ABRB-5			Upper core projection failure	C	At −0.64% in the 6th 1.2% compression excursion
ABRB-6			Upper core projection failure	C	At 0.24% in the 1st 2% compression excursion
ABRB-7			Core rupture	—	At 1.23% in the 6th 3% tension excursion

5. EFFECT OF ABRB DETAILS

5.1. Effect of brace end rotation

As is shown in Figure 15, the rotation demands of ABRB-1 and ABRB-4∼ABRB-6 were greater than those of ABRB-2, ABRB-3 and ABRB-7. In addition, core projection failure was successfully prohibited for the specimens with less significant end rotation response. It indicates that end rotation has a significant effect on the seismic behavior of BRBs. It also shows that incorporating rotation restraint at the brace ends is an effective way to minimize the brace end rotation demand and avoid core projection failure for hinge-type BRBs.

It should be noted that the authors do not intend to promote the rigid connection although it showed much better performance than hinge connection in this study. The reason is that the rigid connection for ABRB-3 and ABRB-7 cannot simulate the real boundary condition for the

DOI: 10.1002/eqe

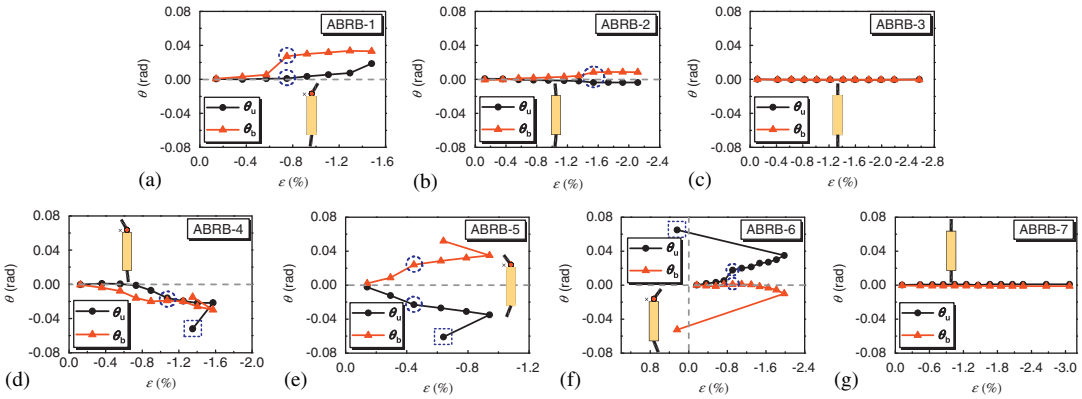

Figure 15. Development of brace end rotation demand of ABRB specimens.

BRBs with bolted brace-to-gusset plate connections since the real frame action in such BRBF will also induce brace end rotation on the BRBs. Therefore, the negative effect of brace end rotation on the seismic behavior of BRBs with either bolted brace-to-gusset plate connections or hinge connections should be taken into account.

5.2. *Effect of core-type detail*

The effect of core type detail is examined between ABRB-3 (core type A) and ABRB-7 (core type B). The test results indicate that the core type A with the abrupt varied cross-section as a stopper caused a much more severe stress concentration on such abrupt varied cross-section This led to the earlier core rupture at the core strain of 2.05% for ABRB-3. On the other hand, the core of ABRB-7 did not rupture until the 6th 3% tension excursion, and the CPD and CPE of ABRB-7 are almost 1.7 times those of ABRB-3, which indicates that the stopper in core type B with the gradual varied cross-section can ensure much better cyclic behavior and much higher low-cycle fatigue property.

6. ANALYSIS OF CORE PROJECTION FAILURE MECHANISM

Although the BRBs (core buckling restrained by concrete-filled steel tube) with hinge connections to the gusset plates showed good seismic behavior in the brace–beam–column connection of BRBF [21], the test in this study showed that significant rotation response might develop at the brace ends, and core projection failure were prone to occur for the BRBs with greater end rotation. Especially, core projection failure still occurred even though its cross-section was reinforced by stiffening plates two times that of the yielding segment for ABRB-1. This is a conventional constructional detail for the core projection of BRBs and could ensure elastic response within the core projection segment for ABRB-1 under axial loading, because the peak overstrength factor for this specimen was only 1.53. It is also clear from the test results that the rotation restraint is an effective way to minimize brace end rotation. However, it may not be a cost-effective way because such a configuration will also increase the total steel consumption of BRBs. For these reasons, a deeper discussion on the core projection failure mechanism is still needed to ensure proper seismic behavior of BRBs.

6.1. *Analytical model*

The rotation models and development of core projection failure are presented in Figures 16 and 17, respectively. The connectors and external restraints are regarded as rigid body in this model for their high flexural stiffness. In addition, the minor flexural deformation of the core projection

DOI: 10.1002/eqe

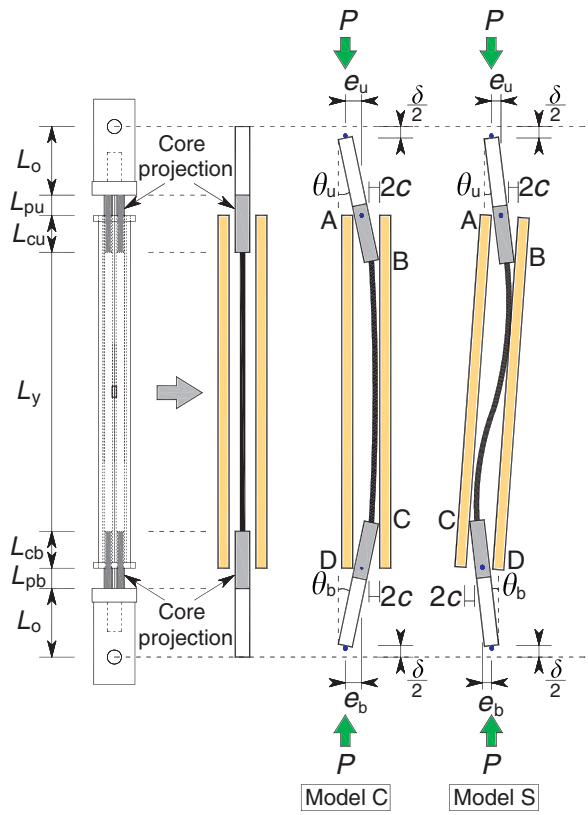

Figure 16. Two rotation models for core projection failure.

segment is neglected because the core projection length is short for all the specimens in the test. Hence, the hinge connector and core projection segment both have the same rotation.

As is shown, when the brace is under compression (δ represents the total axial deformation), both the brace ends are prone to rotate in a certain direction until points A, B or C, D of the core stiffening segment contact with the external restraint with the rigid-body rotation θ_r because of the clearance c between the core and external restraint. During this process, the loading point P will move horizontally relative to the center of the core projection with an additional loading eccentricity e_u and e_b (subscript u and b represent upper and lower brace end, respectively), and hence the core projection will be subjected to a combined axial load and additional bending moment ($P-M$) simultaneously. Such bending moment becomes prominent with the steadily increased brace force and some plastic rotation response will gradually develop when the $P-M$ response causes yielding at the fringe fiber of core projection. In spite of this, the ABRB can still sustain larger axial load without losing its strength. Finally, core projection failure will occur when the $P-M$ response exceeds its interior ultimate strength capacity (N_{ui}, M_{ui}), and a plastic hinge forms at the bottom of the core projection, which will lead to a geometrically unstable system and the declination of strength.

6.2. $P-M$ response

The $P-M$ response at the first compression peak of each strain amplitude is needed to examine the development of stress state in the core projection. As is shown in Figure 16, the brace end rotation demands θ_u and θ_b were measured directly in the test by the LVDT displacement transducers, hence, the bending moment M_{up} at the upper end and M_{low} at the lower end can be obtained as follows based on the small deformation theory, in which the initial eccentricity e_i is considered in

DOI: 10.1002/eqe

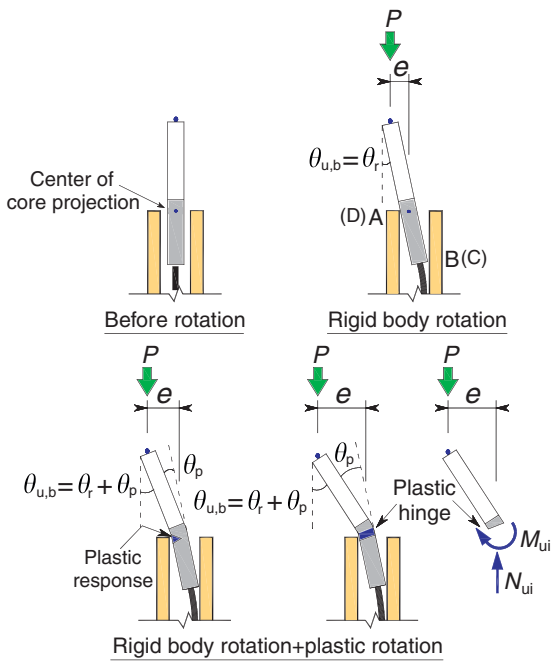

Figure 17. Development of core projection failure.

e_u and e_b for ABRB-5:

$$M_{\text{up}} = Pe_u = P\theta_u(L_{\text{o}} + L_{pu} - \delta/2) \tag{10}$$

$$M_{\text{low}} = Pe_b = P\theta_b(L_{\text{o}} + L_{pb} - \delta/2) \tag{11}$$

The normalized $N_u - M_u$ correlation curves along with the non-dimensional $P - M$ responses are presented in Figure 18 (incomplete plot for ABRB-1 for the acquisition error). The dashed square denotes the combined response when core projection failure occurred. It is clear that the bending moment response for specimen ABRB-1, ABRB-4∼ABRB-6 developed significantly with the steadily increased strain amplitude. Of these specimens, most of the $P - M$ responses remained within elastic region at small strain amplitude. However, such combined responses gradually developed into the plastic region, and finally core projection failure (marked with dashed square) occurred only if the $P - M$ response exceeded the corresponding ultimate strength, indicating that plastic hinge formed at this moment. Furthermore, the bending moment at the upper end was relatively more significant than that at the lower end especially for ABRB-4∼ABRB-6 when failure occurred, and this also explains the reason for the upper end failure. On the other hand, the core projections of ABRB-3, ABRB-7 and ABRB-2 were all kept within elastic stage under all strain amplitudes, and the bending moments were much less significant than those of the other specimens. This indicates that the core projection failure mode can be successfully prohibited if brace end rotation is minimized and the core projection is always kept within elastic stage under the most unfavorable $P - M$ response. It can be concluded from the analysis above that the bending moment response induced by the brace end rotation should be considered into core projection design.

It is clear from the failure mode analysis that the bending moment response developed in the core projection is mainly determined by brace end rotation demand. Such an end rotation is also related to the brace end connection details (hinge or bolted connection) and interaction between the core stiffening segment and external restraint. Although a few studies [22–24] have been conducted on this issue, most of them only focused on the BRBs with bolted connections and ignored possible contact interaction near the ends of external restraint and the effect of gap. However, the analysis

DOI: 10.1002/eqe

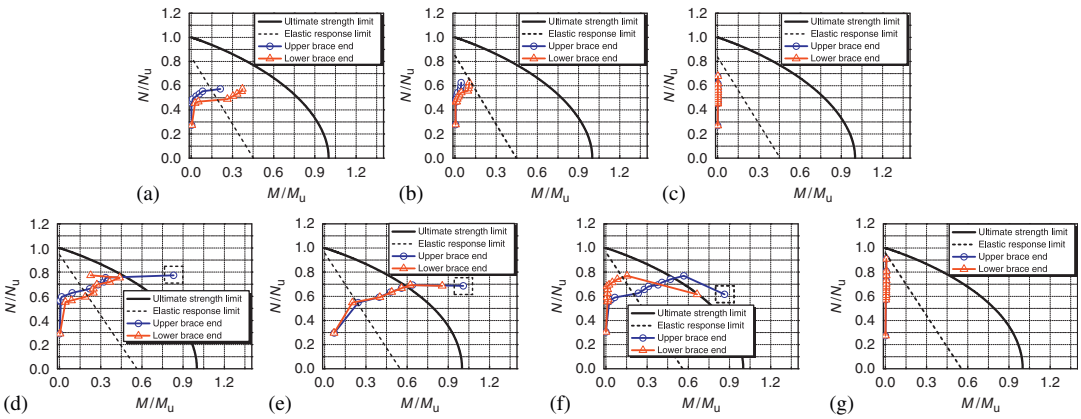

Figure 18. Normalized $N_u - M_u$ correlation curve and $P - M$ response: (a) ABRB-1; (b) ABRB-2; (c) ABRB-3; (d) ABRB-4; (e) ABRB-5; (f) ABRB-6; and (g) ABRB-7.

in this study shows that the presence of gap seems to be related to the end rotation demand, which may be more unfavorable to the stability of core projection of pin-connected BRBs. In addition, two end rotation modes were also observed in this test and few related discussions have been reported especially for BRBs with pinned connections. In view of this, further research is needed to gain further insight into core projection design by considering the effect of connection details, gap, end rotation models and contact interaction near the casing ends.

7. CONCLUSIONS

A novel type of angle steel buckling-restrained brace (ABRB) that enables easier control on the initial geometric imperfection in the core, more design flexibility in the buckling restraining mechanism and easier assembly has been developed.

Component test on seven ABRB specimens was conducted and the test results indicate that the absence of welding within the core can help to minimize the initial geometric imperfection, ensure consistency between design and actual member quality, and improve the low-cycle fatigue property of the core. The ABRBs exhibited stable and repeatable cyclic behavior, and showed satisfactory cumulative plastic ductility (CPD) capacity with the peak core strain of 3% and peak CPD capacity of 1068, which shows that ABRBs can serve as effective hysteretic dampers for engineering structures.

Core projection failure was found to be the primary failure mode for the ABRBs with hinge connections. The test results show that brace end rotation are a most crucial factor on such a failure mode, and earlier core projection failure occurred for the ABRBs with greater brace end rotation demand, which highlights the importance to minimize such a rotation and consider this effect in design of core projection. Based on the failure mechanism analysis, it is suggested that the core projection should be kept within elastic stage under the possible maximum $P - M$ response to ensure proper seismic behavior.

More details concerning the influential factors on the compression-flexure failure mode of ABRBs and the design criteria for steel core projection considering the $P - M$ response are to be further discussed in a companion paper in progress.

ACKNOWLEDGEMENTS

The project was financially supported by the National Basic Research Program of China (973 Program) (2007CB714204) and the National Key Technology R&D Program (2006BAJ03B06-01, 2006BAJ06B03-03). The authors also express great thanks to Dr Yubin Tian, Mr Yunfei Ma and other laboratory personnel

DOI: 10.1002/eqe

at the Structural and Seismic Testing Center, Harbin Institute of Technology, China for their assistance during the test.

REFERENCES

1. Xie Q. State of the art of buckling-restrained braces in Asia. *Journal of Constructional Steel Research* 2005; **61**:727–748.
2. Uang CM, Nakashima M, Tsai KC. Research and application of buckling-restrained braced frames. *International Journal of Steel Structures* 2004; **4**:301–313.
3. Watanabe A, Hitomi Y, Saeki E, Wada A, Fujimoto M. Properties of brace encased in buckling-restraining concrete and steel tube. *Proceeding of the 9th World Conference on Earthquake Engineering*, Tokyo, vol. IV, 1988.
4. Iwata M, Murai M. Buckling-restrained brace using steel mortar planks; performance evaluation as a hysteretic damper. *Earthquake Engineering and Structural Dynamics* 2006; **35**:1807–1826.
5. Inoue K, Sawaizumi S, Higashibata Y. Stiffening requirements for unbonded braces encased in concrete panels. *Journal of Structural Engineering* (ASCE) 2001; **127**:712–719.
6. Ding YK, Zhang YC, Zhao JX. Tests of hysteretic behavior for unbonded steel plate brace encased in reinforced concrete panel. *Journal of Constructional Steel Research* 2009; **65**:1160–1170.
7. Nagao T, Takahashi S. A study on the elasto-plastic behavior of unbonded composite bracing (part 1 experiments on isolated members under cyclic loading). *Journal of Structural and Construction Engineering* 1990; **415**:105–115.
8. Satake N, Mase S, Terada T, Isoda K. Development of unbonded brace damper restrained by channel section steel (part 2 static loading test using full-scale specimens). *Summaries of Technical Papers of Annual Meeting*, Architectural Institute of Japan, vol. 9, 2001; 665–666.
9. Murase Y, Morishita K, Inoue K, Tateyama E. Structural design method of the long brace with axial hysteresis dampers at both ends (part 1 analysis on the buckling restraint conditions). *Journal of Structural and Construction Engineering* 2004; **578**:131–138.
10. Ma N, Wu B, Zhao JX, Li H, Ou JP, Yang WB. Full scale test of all-steel buckling restrained braces. *Proceeding of the 14th World Conference on Earthquake Engineering*, Beijing, 2008.
11. Narihara H, Tsujita O, Koeteka Y. The experimental study on buckling restrained braces (part 1 experiment on pin connection type). *Summaries of Technical Papers of Annual Meeting*, Architectural Institute of Japan, vol. 9, 2000; 911–912.
12. Fukuda K, Makino T, Ichinohe Y. Development of brace-type hysteretic dampers. *Summaries of Technical Papers of Annual Meeting*, Architectural Institute of Japan, vol. 8, 2004; 867–868.
13. Newell J, Uang CM, Benzoni G. Subassemblage testing of corebrace buckling-restrained braces (G series). *Report No. TR-06/01*, University of California, San Diego, 2006.
14. Aiken ID, Mahin SA, Uriz P. Large-scale testing of buckling-restrained braced frames. *Proceeding of Japan Passive Control Symposium*, Tokyo Institute of Technology: Japan, 2002.
15. Merritt S, Uang CM, Benzoni G. Subassemblage testing of star seismic buckling-restrained braces. *Report No. TR-2003/04*, University of California, San Diego, 2003.
16. JGJ 99-98. *Technical Specification for Steel Structure of Tall Buildings*, China Building Technology Research Institute, 1998.
17. Tremblay R, Bolduc P, Neville R, Devall R. Seismic testing and performance of buckling-restrained bracing systems. *Canadian Journal of Civil Engineering* 2006; **33**:183–198.
18. American Institute of Steel Construction (AISC). Seismic provisions of structural steel buildings, Chicago, 2005.
19. Iwata M, Katoh T, Wada A. Performance evaluation of buckling-restrained braces in damage-controlled structures. *Proceeding of the Conference on Behavior of Steel Structures in Seismic Areas. STESSA*, Naples, Italy, 2003; 37–43.
20. Koetaka Y, Tsujita O, Narihara H. The experimental study on buckling restrained braces (part 2 experiment on rigid connection type). *Summaries of Technical Papers of Annual Meeting*, Architectural Institute of Japan, vol. 9, 2000; 913–914.
21. Fahnestock LA, Ricles JM, Sause R. Experimental evaluation of a large-scale buckling-restrained braced frame. *Journal of Structural Engineering* (ASCE) 2007; **133**:1205–1214.
22. Shimizu T, Fujisawa K, Uemura K, Inoue K. Design method to prevent buckling of low yield strength steel tube brace and fracturing of joints (part 1: design method and test plan of braced braces). Summaries of Technical Papers of Annual Meeting, Architectural Institute of Japan, vol. 9, 1997; 781–782.
23. Usami T, Kaneko H. Strength of H-shaped brace constrained flexural buckling having unconstrained area at both ends (both ends simply supported). *Journal of Structural and Construction Engineering* 2001; **542**:171–177.
24. Tsai KC, Hsiao PC. Pseudo-dynamic test of a full-scale CFT/BRB frame—part II: seismic performance of buckling-restrained braces and connections. *Earthquake Engineering and Structural Dynamics* 2008; **37**: 1099–1115.

DOI: 10.1002/eqe